Proceedings of the ASME 2007 International Design Engineering Technical Conferences & Computers and Information in Engineering Conference
IDETC/CIE 2007
September 4-7, 2007, Las Vegas, Nevada, USA

DETC2007-34996

THE EFFECT OF HIGH ORDER NON-LINEARITIES ON SUB-HARMONIC EXCITATION WITH PARALLEL PLATE CAPACITIVE ACTUATORS

Alexander A. Trusov*
MicroSystems Laboratory
Dept. of Mechanical and Aerospace Engineering
University of California, Irvine
Irvine, CA 92697-3975
Email: atrusov@uci.edu

Andrei M. Shkel
MicroSystems Laboratory
Dept. of Mechanical and Aerospace Engineering
University of California, Irvine
Irvine, CA 92697-3975
Email: ashkel@uci.edu

ABSTRACT

Electrostatic actuation of motion is commonly used in resonant MEMS. Drive signal feed-through is undesirable as it masks the detection signal. This paper reports analysis and demonstration of a resonant motion excitation scheme, which uses a combination of a DC bias with a sinusoidal AC voltage, frequency of which is twice of the mechanical resonant frequency. This configuration is experimentally demonstrated to excite a gyroscope with a parallel plate drive capacitor into high amplitude periodic vibrations. The feed-through has a frequency higher than the main motional harmonic and thus can be eliminated by simple low pass filtering. Full nonlinear dynamics along with several higher-order approximations are considered. Analysis of the effect of the approximation order on the frequency response accuracy shows that the complete nonlinear equation should be used for modeling of high amplitude actuation. Two distinct types of frequency responses are examined as functions of driving AC and DC voltages and damping.

INTRODUCTION

Several important classes of MEMS devices, such as resonators [1], gyroscopes [2], and chemical sensors [3], rely on resonance phenomenon in their operation. In these devices, resonant motion needs to be actuated, detected, and controlled. Capacitive phenomena are commonly used for transduction in vibratory MEMS devices due to the ease of fabrication, low sensitivity to temperature changes, and other practical advantages [4], [5].

Conventional electrostatic actuation schemes use a combination of DC and AC voltages to excite mechanical motion at the resonant frequency of the structure. This is typically achieved by matching the frequency of the drive AC voltage to the resonant frequency of the device. In this case, the amplitude of motion is dictated by the amplitudes of the driving voltages and the quality factor of the mechanical resonator. For this type of actuation, the electrical drive feed-through from drive to sense electrodes caused by parasitic capacitance has the same frequency content as the mechanical motion. Thus, the motional signal is masked by the feed-through, and intricate detection schemes, such as electromechanical amplitude modulation [6], are required to extract and measure the mechanical response. These factors increase the overall system complexity and limit the performance.

Nonlinearity of parallel plate capacitors presents design opportunities for introducing new electrostatic actuation schemes. Issues of large amplitude parallel plate actuation using a conventional combination of DC and AC voltage were extensively studied, for example in [7–9].

Parametric excitation phenomenon in MEMS was reported in [10]. In its simplest form, parametric excitation using electrostatic parallel plate force is described by a classical linear time variant (LTV) Mathieu equation. Dynamics of a clamped-clamped beam under parametric excitation was studied in [11]

*Address all correspondence to this author.

using small amplitude assumption. The effect of an additional third order term was studied in [12]. An interesting parametrically enhanced harmonic actuation scheme using two separate sets of capacitors and AC voltages was proposed in [13]. Most of the relevant literature studies parallel plate parametric effects using approximate equations of motion.

The focus of this paper is actuation of high amplitude vibrations in capacitive MEMS using a combination of a DC bias with a single AC sinusoidal voltage, frequency of which is twice of the mechanical resonant frequency. In Section 1 we introduce a general electro-mechanical model of a MEMS resonator with parallel plate actuation and derive the equations of motion. The phenomenon of high amplitude parametric excitation is demonstrated experimentally in Section 2 using a prototype of a capacitive MEMS gyroscope. In Section 3 we define two different norms of solutions used for frequency response analysis for the nonlinear system. Section 4 presents a comparative numerical study of system dynamics using the complete nonlinear model and its several finite order approximations. Section 5 summarized the obtained results.

1 PARAMETRIC EXCITATION

Figure 1 shows a general schematic of a capacitive micro-resonator, a basic element of various micro-sensors. The electro-mechanical diagram includes the mechanical resonator and the electrostatic drive and sense electrodes. Mass m of the resonator is suspended by a spring k and is constrained to move only along the horizontal x-axis. The variable sense capacitance is defined as $C_s(x)$, and the drive capacitance as $C_d(x)$, where x is the displacement. Typically in MEMS devices, the drive and sense terminals are not completely insulated, but are electrically coupled by stray parasitic capacitors and resistors [6,14,15]. In this paper we assume, without loss of generality, that the parasitic circuit consists of a single lumped capacitor C_p. An AC driving voltage $V_d(t) = v_d \sin(\omega_d t)$ is applied to the drive electrode, and a DC bias V_{dc} is applied to the mass (voltage values are referenced with respect to a common ground).

The sense capacitor C_s is formed between the mobile mass and the fixed sense electrode. The sense electrode is connected to the inverting input of an operational amplifier which is configured as a trans-impedance amplifier, [16]. Due to motion the sense capacitance $C_s(x)$ changes, causing a flow of motional current $I_s = \frac{d(C_s V_s)}{dt}$, where V_s is the sensing voltage across the sense capacitor. The total pick-up current $I(t) = I_s(t) + I_p(t)$ consists of both the motional and the parasitic feed-through currents and is converted to the final output voltage $V(t)$ with trans-impedance gain $-R$. Parasitic current is induced by the drive voltage V_d and therefore has the same frequency ω_d. The total sensing voltage is the DC bias V_{dc}. According to the laws of electrostatics, the total pick-up current that flows through the feed-back resistor of the trans-impedance amplifier is $I(t) = \frac{d}{dt}[V_d(t)C_p + V_{dc}C_s(t)]$.

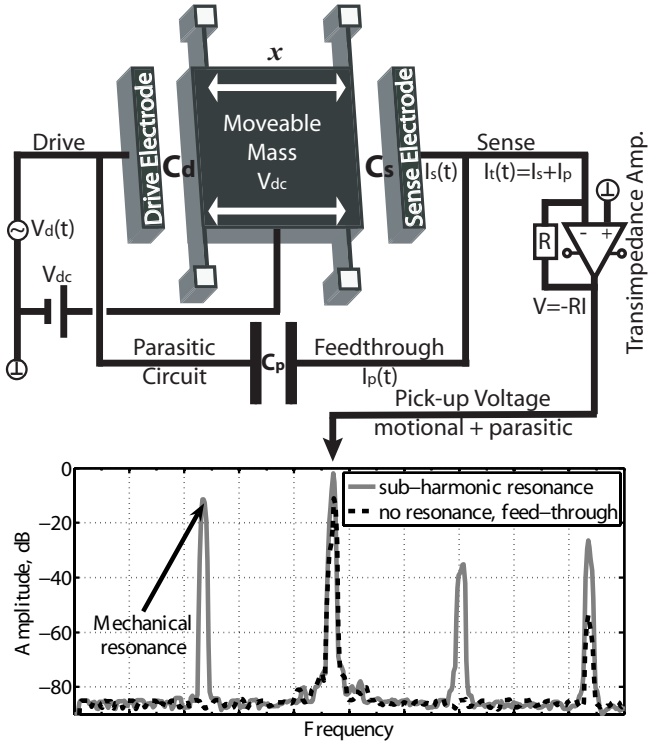

Figure 1. Schematic of a capacitive MEMS resonator with parallel plate sub-harmonic excitation.

Since the parasitic capacitance C_p and the voltage V_{dc} are constant,

$$I(t) = V_{dc}\frac{dC_s(t)}{dt} + C_p\frac{V_d(t)}{dt}. \tag{1}$$

The motion of the resonator is governed by

$$\ddot{x} + \frac{\omega_n}{Q}\dot{x} + \omega_n^2 x = \frac{1}{2m}\frac{\partial C_d(x)}{\partial x}(V_{dc} + V_d(t))^2, \tag{2}$$

where $\omega_n = \sqrt{\frac{k}{m}}$ is the undamped natural frequency and Q is the quality factor. Let us denote the initial gap between plates in the parallel plate driving capacitor at rest by g, the overlap length of individual parallel plate pairs by L, height of the plates (i.e. structural layer thickness) by y, and permittivity of the media by ε. The total overlap area in the drive capacitor is given by $A = NLy$, where N is a number of parallel plate pairs in the drive capacitor. Then, the variable drive capacitance is

$$C_d(x) = \frac{\varepsilon A}{g - x} = \frac{\varepsilon A}{g}\frac{1}{1 - x/g}. \tag{3}$$

We introduce the nominal drive capacitance $C_{dn} = \varepsilon A/g$ and gap-normalized dimensionless displacement $\chi = x/g < 1$. From Eqn. (3), using Taylor series expansion with respect to $\chi \approx 0$, the drive capacitance is

$$C_d = C_{dn}\frac{1}{1-\chi} = C_{dn}\sum_{n=0}^{\infty}\chi^n. \quad (4)$$

The electrostatic force produced by the drive capacitor is proportional to the gradient of the capacitance

$$\frac{\partial C_d}{\partial x} = \frac{\partial}{\partial x}\left(\frac{C_{dn}}{1-\chi}\right) = \frac{C_{dn}}{g}\frac{1}{(1-\chi)^2} = \frac{C_{dn}}{g}\sum_{n=0}^{\infty}(n+1)\chi^n. \quad (5)$$

Finally, from Equations (2) and (5), normalized displacement χ of the resonator is governed by

$$\ddot{\chi}(t) + \frac{\omega_n}{Q}\dot{\chi}(t) + \omega_n^2\chi(t) = \frac{C_{dn}}{2mg^2}(V_{dc}+V_d)^2\frac{1}{(1-\chi)^2}, \quad (6)$$

or equivalently, by

$$\ddot{\chi}(t) + \frac{\omega_n}{Q}\dot{\chi}(t) + \omega_n^2\chi(t) = \frac{C_{dn}}{2mg^2}\sum_{n=0}^{\infty}(n+1)\chi^n \times \quad (7)$$
$$\times\left\{(V_{dc}^2+\frac{1}{2}v_d^2) + 2V_{dc}v_d\sin(\omega_d t) - \frac{1}{2}v_d^2\cos(2\omega_d t)\right\}.$$

This equation has a nonlinear and time dependent right hand side. The nonlinearity is due to the parallel plate capacitance gradient, Fig. 2; the voltage-square term causes the time dependency of the excitation. Let us consider several special cases.

A linear time invariant (LTI) approximate model can be obtained by neglecting the linear time-dependent and the nonlinear terms on the right hand side. The resulting model is identical to the case of classical lateral comb actuation. For this model, the resonant motion can be achieved in the following two cases: driving AC voltage $v_d(t)$ is applied at the resonance frequency or at its half. In the first case, $\omega_d \approx \omega_n$ and the forcing term $\frac{C_{dn}}{mg^2}V_{dc}v_d sin(\omega_d t)$ provides resonant excitation. In the second case, $\omega_d \approx \frac{1}{2}\omega_n$ and $\frac{C_{dn}}{4mg^2}v_d^2 cos(2\omega_d t)$ provides resonant excitation. The drawback of $\omega_d \approx \omega_n$ is that motion and parasitics occur at the same frequency. The main disadvantage of $\omega_d \approx \omega_n/2$ is the low actuation gain, caused by the $\frac{1}{2}v_d^2$ coefficient.

The next level of approximation can be obtained in the following way. First, we assume $\|V_{dc}\| \gg \|V_d\|$ and neglect terms proportional to v_d^2. Second, we linearize the capacitance gradient

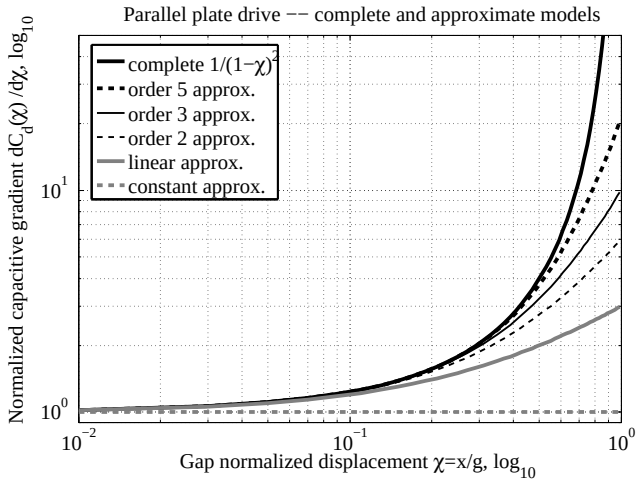

Figure 2. Nonlinear capacitive gradient of parallel plates and its finite order approximations.

using Eqn. (5) as $\frac{\partial C_d}{\partial x} \approx \frac{C_{dn}}{g}(1+2\chi)$. Finally, Eqn. (7) is simplified to

$$\ddot{\chi}(t) + \frac{\omega_n}{Q}\dot{\chi}(t) + \omega_n^2\chi(t) = \frac{C_{dn}}{2mg^2}\left\{V_{dc}^2 + 2V_{dc}v_d\sin(\omega_d t)\right\}(1+2\chi), \quad (8)$$

which is equivalent to

$$\ddot{\chi}(t) + \frac{\omega_n}{Q}\dot{\chi}(t) + \left(\omega_n^2 - \frac{V_{dc}C_{dn}}{mg^2}\left[V_{dc} + 2v_d\sin(\omega_d t)\right]\right)\chi(t) =$$
$$= \frac{V_{dc}C_{dn}}{2mg^2}\left[V_{dc} + 2v_d\sin(\omega_d t)\right]. \quad (9)$$

This equation (obtained by neglecting v_d^2 and linearization with respect to χ) is very similar to the classical Mathieu equation [10], which describes zero-input parametric instability, caused by harmonic modulation of the effective stiffness. However, Eqn. (9) is not homogenous and is simultaneously forced with a static force and a sinusoidal force at ω_d frequency. This equation, common in MEMS literature on parallel plate actuation [10], qualitatively explains two phenomena inherent to parallel-plate actuation: active resonant frequency tuning and parametric resonance.

The effective natural frequency for a parallel-plate actuated motion is given by $\left(\omega_n^2 - \frac{V_{dc}C_{dn}}{mg^2}\left[V_{dc} + 2v_d\sin(\omega_d t)\right]\right)$. The stiffness reduces quadratically with applied DC bias as $k\left(\omega_n^2 - \frac{C_{dn}}{mg^2}V_{dc}^2\right)$. This effect is known as frequency tuning and the corresponding mathematical model is known as negative

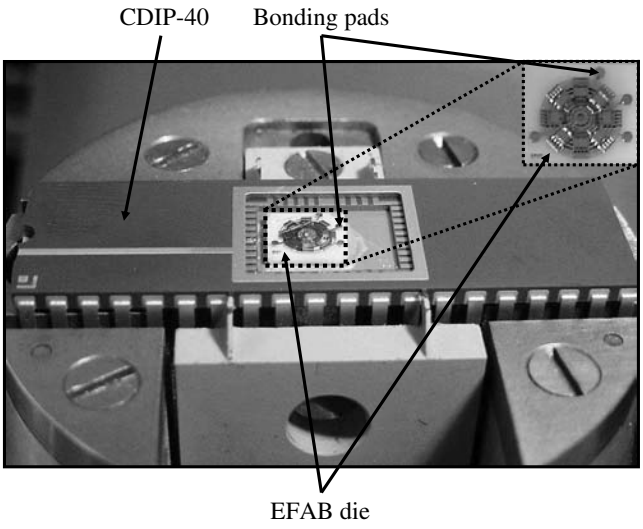

Figure 3. Packaged prototype of distributed mass gyroscope (DMG) fabricated in EFAB process.

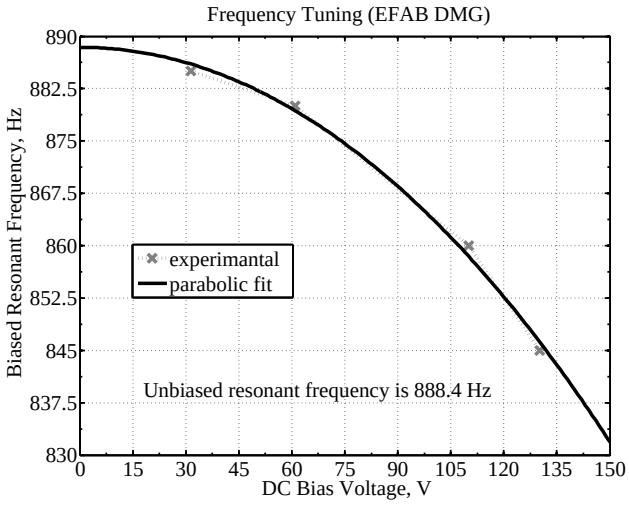

Figure 4. Characterization of parallel plate frequency tuning in the device.

electrostatic spring. In Section 2 frequency tuning of a MEMS gyroscope prototype is experimentally characterized.

Classical parametric resonance is a property of a linear time-varying dynamic system to develop unstable motion from non-trivial initial conditions under harmonic modulation of the effective stiffness. Parametric resonance for both non-damped and damped systems governed by Mathieu equation is a well studied problem – in both cases motion with infinitely growing amplitude occurs when the stiffness modulation frequency satisfies the condition $\omega_d = \frac{2}{k}\omega_n$, $k = 1, 2, ..., \infty$. The case of $k = 1$, $\omega_d = 2\omega_n$, is of the greatest practical interest, because it is the only k for which the frequency of the feed-through is above the frequency of motion. Feasibility of this scheme of excitation is experimentally studied in Section 2. Numerical analysis of different order approximations of Eqn. (7) is presented in Section 4.

2 DEMONSTRATION OF SUB-HARMONIC EXCITATION

The simplified LTV approximation given by Eqn. (9) allows to predict phenomenon of parametric resonance in parallel plate actuated MEMS. Specifically, we can expect the system to develop significant amplitudes of motion, when driving AC voltage is applied at double of the resonant frequency (taking into account frequency down-tuning due to the DC voltage). The motion occurs at the tuned resonant frequency, which is half of the driving AC voltage frequency. In this section we experimentally characterize this nonlinear actuation method.

2.1 Test-Bed

A prototype of a Distributed Mass Gyroscope (DMG) [15] was used for experimental demonstration of parametric actuation. The device was fabricated using EFAB^{TM} [17], a commercial process from Microfabrica. The core of the EFAB process is a sequential electrodeposition of multiple structural layers. Square dies (5×5) mm were formed on 0.5 mm thick alumina (Al_2O_3) substrate. The first 10 μm thick Ni-Co structural layer was deposited using electroplating and patterned. Then, blanket Cu layer was electroformed and planarized to the thickness of the structural layer. The cycle of these two steps was repeated 20 times, after which the sacrificial Cu layer was chemically etched away. As a result, a 200 μm high 3D metal structures on a non-conductive substrate were formed. For the fabricated gyroscope, the minimal line-width was 20 μm and minimal spacing was 30 μm.

Figure 3 shows a packaged and wire-bonded device. The drive mode of the gyroscope was used in this paper to study high amplitude actuation based on nonlinear parametric resonance phenomenon.

2.2 Structural Characterization

In order to characterize frequency tuning and the unbiased natural frequency of the device, resonance was visually detected at different values of V_{dc}. Figure 4 shows the collected data along with the curve fitting results. Structural properties of the device were also characterized in air and in vacuum using electrostatic method of parasitics-free half-frequency sweep [15]. Figure 5 shows the experimental data and the curve fitting results. The resonant frequency was 878 Hz for a DC bias of 60 V; the quality factor was 275 in air and 860 in 200 mTorr vacuum.

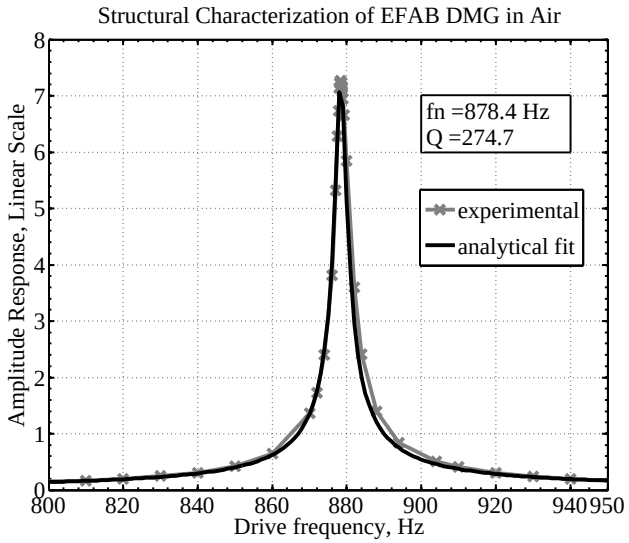

(a) In air

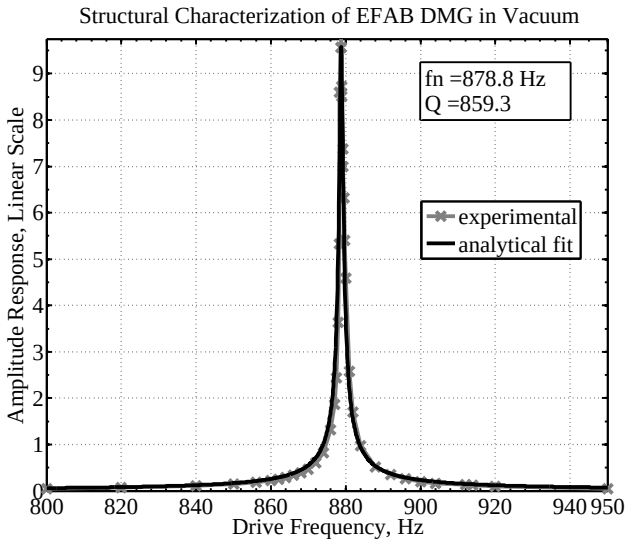

(b) In 200 mTorr vacuum

Figure 5. Structural characterization of the device using electrostatic actuation and capacitive detection.

2.3 High Amplitude Parametric Resonance

Nonlinear parametric excitation of motion at resonant frequency by a twice higher frequency AC voltage is experimentally characterized in this section. This actuation method provides high amplitude of motion and robustly separates motion from the parasitics in frequency domain.

The experimental setup consisted of a packaged gyroscope assembled on a breadboard together with a trans-impedance amplifier. The tested mode of vibration was characterized utilizing parallel plate actuation and sensing, as shown in Fig. 1. The capacitive gap between 20 μm wide parallel plates was 30 μm. The DC bias voltage was applied to the body of the resonator. The driving AC voltage was imposed onto the anchored parallel plate structure. Sensing of the motion was done using anchored parallel plate structure, which was virtually grounded by means of trans-impedance amplifier with a 1 MΩ feedback resistor. The sense capacitor between fixed and moveable parallel plates had a fixed DC voltage difference across it. Velocity dependent motional current flows through the feedback resistor of the trans-impedance amplifier. Also, capacitive coupling between drive and sense electrode contributes to the output current. The total pick-up current was converted to voltage and fed into a signal analyzer HP 35665A for spectral analysis and data capturing.

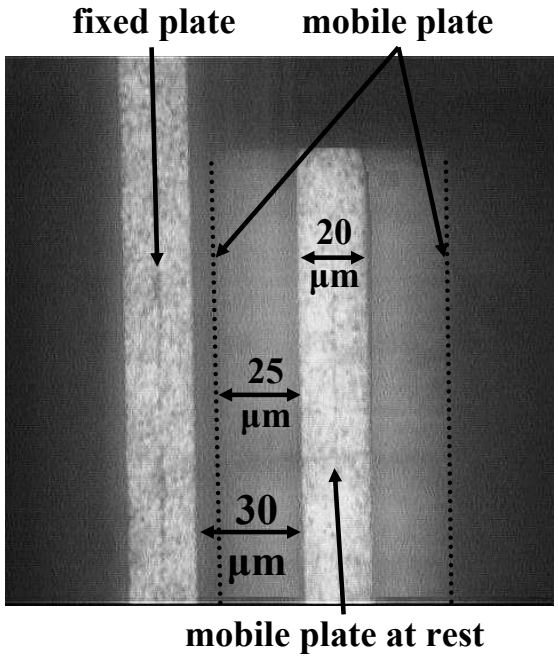

Figure 6. Superimposed optical photographs of parallel plate device at rest and at resonant motion parametrically excited by a twice higher frequency AC voltage. The blurred area shows amplitude of motion ($\approx$80% of the gap).

During the experiments, the ω_d frequency of the driving AC voltage $V_d(t)$ was manually swept in the vicinity of $2\omega_n$. The amount of motion was detected visually using a microscope, Fig. 6. At the same time, the Fast Fourier Transform (FFT) of the pick-up signal was continuously performed, updated, displayed and stored by the dynamic signal analyzer. We compared results of the FFT at resonance and off-resonance (in our experimental setup this means that motional amplitudes were smaller than optically resolvable $\approx 0.25\mu$m). From this comparison, shown in Fig. 7, we determined the frequency content of the feed-through signals and distinct features of the pick-up signal in the presence of parametrically excited motion.

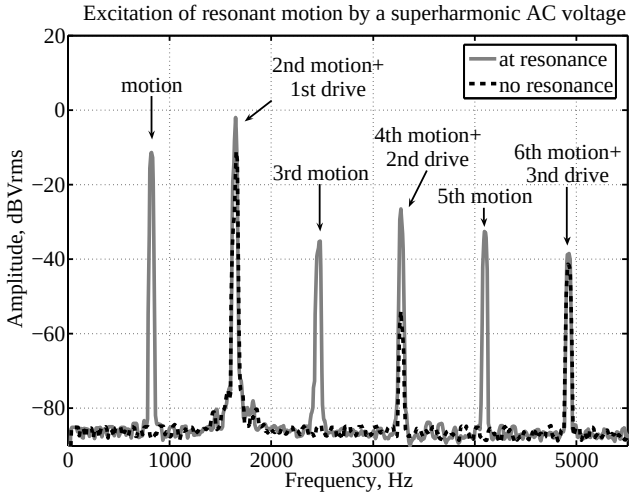

Figure 7. Experimental pick-up signal PSD for parametrically excited resonator. The driving AC voltage is provided at double of the resonant frequency. The strong frequency separation between first (main) motional component and parasitics is achieved.

We registered the large amplitude of motion when the driving AC voltage was applied at frequency close to twice of the DC tuned resonant frequency (i.e. $\omega_d \approx 2\omega_n$, $f_d \approx 2*850 = 1.7$ kHz). The amplitude of motion was several times higher than in the case of conventional LTI excitation (i.e. $\omega_d \approx \omega_n$) using the same combination of DC and AC voltages. Due to the capacitive parasitic coupling and non-ideality of the AC voltage generator, the feed-through of the drive occurs at all multiple harmonics of the driving AC frequency (i.e. at $n*1.7 = 1.7, 3.4, 5.1, ...$ kHz). In other words, the drive voltage leakage is present at all even order multiples of the resonant frequency. However, the motion mainly occurs at the resonant frequency. Thus, the main vibrational mode is sub-harmonic with respect to the driving AC voltage. In addition to the main mode at the resonant frequency, the motion also occurs at the resonant frequency and all of its multiples (i.e. at $n*0.85 = 0.85, 1.7, 2.55, 3.4, 4.25, 5.1, ...$ kHz).

To conclude, nonlinear parametric excitation of resonant motion by a higher frequency voltage was demonstrated using a parallel plate actuated device. This non-LTI actuation approach experimentally exhibits several important advantages over the conventional LTI driving schemes. The advantages include actuation of large amplitudes of motion (80% of the gap) using relatively small voltages, and robust frequency separation between the motion and the drive AC voltage feed-through. Parametric excitation of periodic resonant motion by a higher frequency AC voltage can potentially be used to provide resonant devices with wider bandwidth and higher gain while simplifying the detection of motion.

3 FREQUENCY RESPONSE NORMS

Small amplitude parametrically excited motion can be modeled by classical Mathieu equation [10]. The focus of this paper, however, is the steady-state large amplitude vibrations excited using parallel plate capacitors. Parametric excitation of large amplitude vibrations was experimentally demonstrated in Section 2. In this section we model and analyze the dynamics using the complete Eqn. (7) along with several orders of approximations. These models of the dynamics can be uniformly described by

$$\ddot{\chi}(t) + \frac{\omega_n}{Q}\dot{\chi}(t) + \omega_n^2\chi(t) = \frac{C_{dn}}{2mg^2}\sum_{n=0}^{N}(n+1)\chi^n \times \qquad (10)$$
$$\times \left\{ (V_{dc}^2 + \frac{1}{2}v_d^2) + 2V_{dc}v_d\sin(\omega_d t) - \frac{1}{2}v_d^2\cos(2\omega_d t) \right\},$$

where N defines the order of the Taylor sum approximation for the nonlinear capacitive gradient on the right hand side. Order $N = 1$ corresponds to the often used LTV model, while infinite summation corresponds to the complete nonlinear model of $\partial C_d(\chi)/\partial\chi = 1/(1-\chi)^2$.

Equation (10) was solved numerically in the complete nonlinear form along with $N = 1, 2, 3, 5$ order approximations using integration routine *ode*45 in MATLAB. Based on the sensitivity analysis, the time increment was set to 10^{-2} of the resonant vibrations period to ensure precision of the numerical solutions. The total solution time interval was 1 s. The output of the code was a multi-dimensional array of time domain solutions, corresponding to different orders N and values of the system parameters.

Frequency responses were calculated from the steady-state response parts of the time domain solutions by a separate MATLAB code. It is important to explicitly define the notion of the frequency response, since for the non-LTI system described by Eqn. (10) the motion occurs at an infinite number of frequencies. We define two alternative norms of the $\chi(t)$ solutions for a given drive AC frequency ω_d: $\|\chi(t)\|_{max}$ and $\|\chi(t)\|_{\left(\frac{\omega_d}{2}\right)}$. The total amplitude of motion norm $\|\chi(t)\|_{max}$ is defined as the maximum span of $\chi(t)$ on a certain time interval. This norm determines if the solution is bounded and physically feasible. This approach to frequency response analysis is typically used to study instability conditions of parametrically excited micro-resonators, for example [11].

Operation of many resonant MEMS sensors, however, is based on a certain mode of vibration. For instance, in vibratory gyroscopes the input angular rate stimulus is amplitude-modulated and subsequently detected at the frequency of the resonant vibrational mode. If parametric phenomenon is used to actuate such devices, the amplitude of only the main resonant motion harmonic defines the scale factor and other performance

characteristics of the device. Therefore, for micro-devices based on sinusoidal motion and Fourier signal processing, a different definition of norm should be used to study frequency responses. This norm is the amplitude of the sinusoidal component of the motion at the resonant frequency. In other words, $\|\chi(t)\|_{(\frac{\omega_d}{2})}$ is the norm of the orthogonal projection of $\chi(t)$ onto the Fourier basis function $e^{i\frac{\omega_d}{2}t}$, i.e.

$$\|\chi\|_{(\frac{\omega_d}{2})} = \frac{\|\int_{t_0}^{t_1} \chi(t) e^{(i\frac{\omega_d}{2}t)} dt\|}{\|\int_{t_0}^{t_1} e^{(i\omega_d t)} dt\|}. \quad (11)$$

To summarize, two different types of frequency response analyses were numerically studied for a parametrically excited micro-device. It was concluded, that drive frequency ω_d dependency of $\|\chi(t)\|_{max}$ describes the instability regions, while $\|\chi\|_{(\frac{\omega_d}{2})}$ defines performance characteristics of sinusoidal motion based resonant micro-devices.

4 MODELING OF NON-LINEARITIES

In this section we discuss the results of dynamics modeling. The model of the resonator is based on the device, which was characterized in Section 2; the device has the following nominal parameters: $f_n = 850\ Hz$, $Q = 270$, effective $m = 9.3e\text{-}7\ kg$, $C_{dn} = 0.5\ pF$, $V_{dc} = 20\ V$, $v_d = 5\ V_{pk}$.

4.1 Effect of Approximation Order

Figure 8(a) shows $\|\chi\|_{max}$ frequency responses of the resonator, obtained using $N = 1,2,3$ order approximations of Eqn. (10) and a complete nonlinear model. Mathieu equation type LTV model shows classical unbounded parametric resonance, which is different from experimentally observed high amplitude vibration; the frequency domain instability region given by this model is also different from the actual.

Second order model shown in Fig. 8(a) is also quantitatively different from the complete model, however the predicted resonant region is very close to the actual. Third order model is close to the actual, however the amplitude of the total $\|\chi\|_{max}$ response is overestimated. In general, finite order N approximations of Eqn. (10) result in overestimated amplitudes of motion; amount of the overestimation reduces with higher order approximation order N.

Figure 8(b) shows a comparison between $\|\chi\|_{max}$ and $\|\chi(t)\|_{(\frac{\omega_d}{2})}$ frequency responses for a complete model and a third order approximation. The frequency domain resonant regions coincide, and the profiles of response curves are similar. Most of the motion is produced by a harmonic at $\|\chi(t)\|_{(\frac{\omega_d}{2})}$ frequency. The harmonic frequency responses do not exhibit a characteristic peak, which is observed in the total amplitude frequency response.

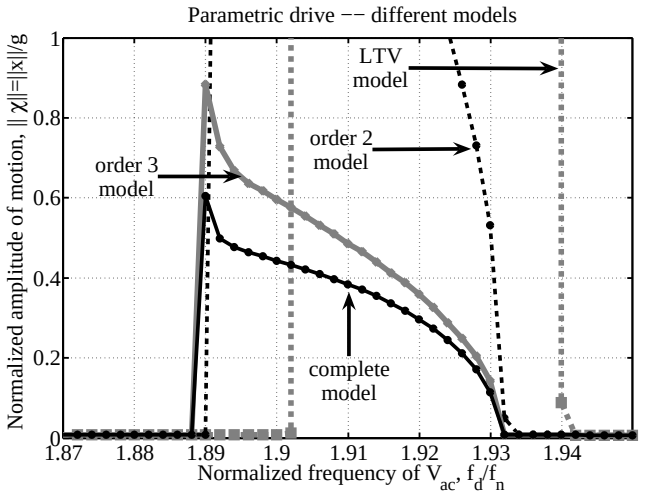

(a) Maximum amplitude of motion $\|\chi(t)\|_{max}$.

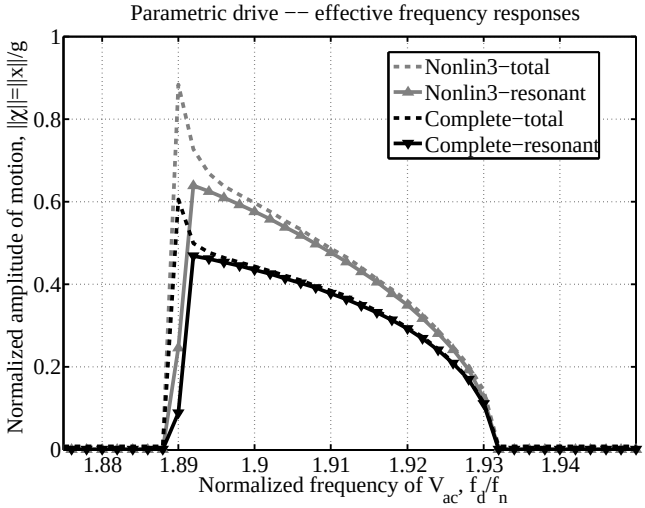

(b) Comparison of $\|\chi(t)\|_{max}$ and $\|\chi(t)\|_{(\frac{\omega_d}{2})}$ frequency responses.

Figure 8. Frequency responses of parametrically excited vibrations defined by two different norms of solutions.

4.2 Effect of AC Drive Voltage Amplitude v_d

Figure 9 shows $\|\chi(t)\|_{(\frac{\omega_d}{2})}$ frequency responses of the resonator for different AC driving voltages $v_d = 2,3,4,5,8,12\ V$ based on the complete model. Depending on the amplitude of the driving AC voltage, there are three regimes of the dynamics.

For small AC amplitudes (in this case, approximately below 1 V), there is no parametric resonance. For a range of voltages (in this case, approximately between 1 and 6 V), there is a well pronounced high amplitude pass-band with a sharp transi-

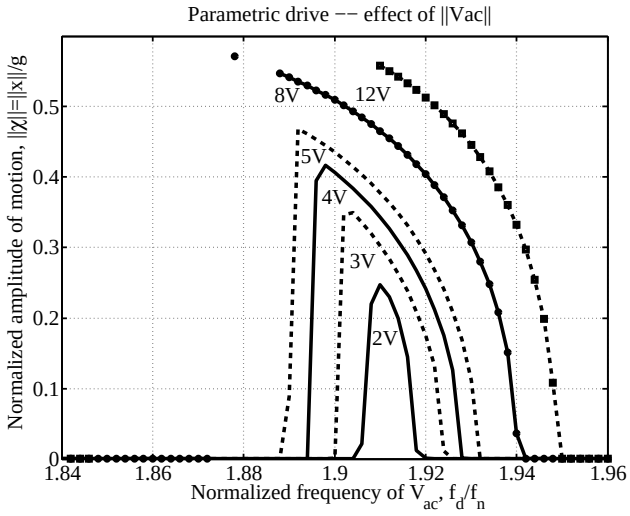

Figure 9. Resonant harmonic frequency response $\|\chi(t)\|_{\left(\frac{\omega_d}{2}\right)}$ for parametric excitation. Effect of the AC driving voltage amplitude.

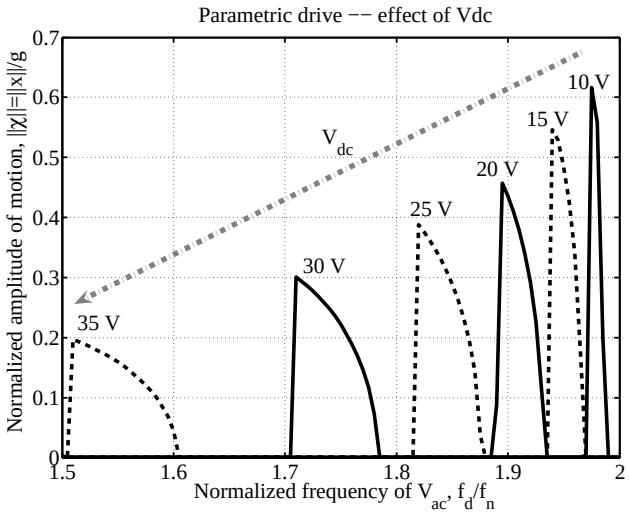

Figure 10. Resonant harmonic frequency response $\|\chi(t)\|_{\left(\frac{\omega_d}{2}\right)}$ for parametric excitation. Effect of the DC bias.

tion on the left side and a smooth slope on the right side. Finally, for voltages above a certain bifurcation threshold, the pass-band breaks into two different regions. The left part of the pass-band shows instability, while the right part allows for stable high amplitude motion. This behavior is specific to the complete nonlinear model of parallel plate parametric excitation.

4.3 Effect of DC Bias Voltage V_{dc}

Figure 10 shows the effect of the DC bias on the $\|\chi(t)\|_{\left(\frac{\omega_d}{2}\right)}$ frequency response. As expected from the negative electrostatic spring effect, the pass-band shifts to the left with increasing V_{dc}. Additionally, the pass-band becomes wider and shorter. This is due to the reduction of the effective parallel plate gap, caused by the static displacement of the mass in response to the DC force.

4.4 Effect of Quality Factor Q

In classical Mathieu equation, damping is known to define parametric instability regions without saturating the amplitude of motion [10]. Figure 11 shows the effect of Q-factor, or, equivalently the damping, on the $\|\chi(t)\|_{\left(\frac{\omega_d}{2}\right)}$ frequency response of a complete nonlinear parallel plate model. Frequency response has a low sensitivity to the quality factor in the wide range of values $10^2 - 10^4$. This relaxes packaging requirements for parametrically actuated devices [11]. Quality factors in the range of $10^2 - 10^3$ are typical of vibratory gyroscopes in air and appear favorable for the parametric excitation.

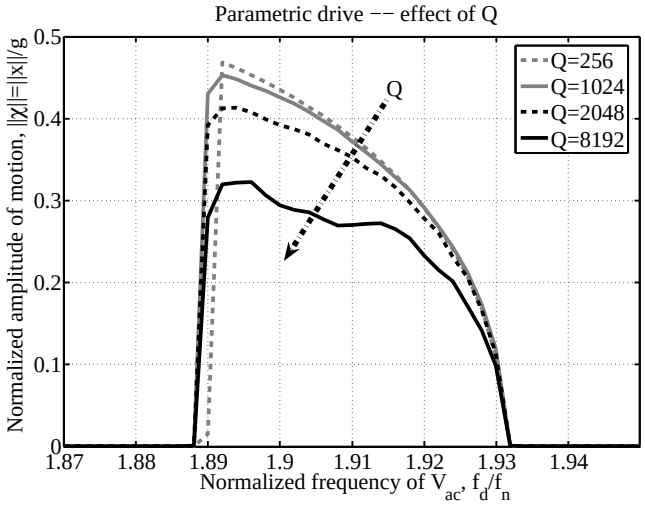

Figure 11. Resonant harmonic frequency response $\|\chi(t)\|_{\left(\frac{\omega_d}{2}\right)}$ for parametric excitation. Effect of the quality factor Q.

5 CONCLUSIONS

In this paper we studied high amplitude actuation of capacitive vibratory devices using parametric resonance. The actuation scheme uses a simple combination of a DC bias with a sinusoidal AC voltage, frequency of which is twice of the resonator's resonant frequency. Experiments demonstrate excitation of high amplitude motion in the parallel plate drive mode of a gyroscope. Since motion mostly occurs at half of the driving AC voltage frequency, feed-through signals can be efficiently eliminated by simple low-pass filtering of the pick-up signal. This removes the need for intricate detection methods and simplifies the overall

system design.

In its linear approximation, the phenomenon is represented by a non-homogenous LTV Mathieu equation. This approach can be used to study small amplitude motion and instability conditions. However, it is not adequate for study of large amplitude responses; higher order terms of the parallel plate capacitive gradient need to be taken into account. In this paper we presented a detailed analysis of two types of frequency responses of parametrically driven resonators using the complete nonlinear model. Maximum displacement $\|\chi(t)\|_{max}$ frequency response determines if the solution is bounded and physically feasible. A different type of frequency response, defined as the amplitude of the main sinusoidal motion at half of the AC voltage frequency $\|\chi(t)\|_{(\frac{\omega_d}{2})}$, prescribes the scale factor of such resonant devices as vibratory gyroscopes.

Finite order approximations of the complete nonlinear electro-mechanical dynamics result in significant overestimation of the actual steady-state response amplitude. Also, lower order approximations describe the resonant region of the frequency response imprecisely. The full nonlinear model should be used in order to precisely model the dynamics.

The described actuation approach is insensitive to damping and can be used to improve performance of vibratory gyroscopes and other resonant MEMS by providing high amplitudes of motion using small voltages and simplifying the detection by isolating parasitics at higher frequencies.

ACKNOWLEDGMENT

This research was partially supported by the National Science Foundation Grant CMS-0409923. We would like to acknowledge Cenk Acar for design of the tested device, Microfabrica for the fabrication of the prototypes, and Adam R. Schofield and Professor Faryar Jabbari for discussions.

REFERENCES

[1] Stemme, G., 1991. "Resonant silicon sensors". *IOP Journal of Micromechanics and Microengineering,* **vol. 1**, pp. 113–125.

[2] Yazdi, N., Ayazi, F., and Najafi, K., 1998. "Micromachined inertial sensors". *Proceedings of the IEEE,* **vol. 86 issue 8**.

[3] Turner, K. K., and Zhang, W. "Design and analysis of a dynamic mem chemical sensor". *Proceedings of the American Control Conference 2001, Arlington, VA, USA, June 25 - 27, 2001*.

[4] Baxter, L. K., 1996. *Capacitive Sensors: Design and Applications*. Wiley-IEEE Press.

[5] Kovacs, G. T., 1998. *Micromachined Transducers Sourcebook*. McGraw-Hill.

[6] Cao, J., and Nguyen, C.-C. "Drive amplitude dependence of micromechanical resonator series motional resistance". *Digest of Technical Papers, 10-th International Conference on Solid-State Sensors and Actuators, Sendai, Japan, June 7 - 10, 1999*.

[7] Lu, M. S.-C., and Fedder, G. K. "Closed-loop control of a parallel-plate microactuator beyond the pull-in limit". *Solid-State Sensor, Actuator and Microsystems Workshop, Hilton Head Island, South Carolina, USA, June 2 - 6, 2002*.

[8] Seeger, J., and Boser, B. "Parallel-plate driven oscillations and resonant pull-in". *Solid-State Sensor, Actuator and Microsystems Workshop, Hilton Head Island, South Carolina, USA, June 2 - 6, 2002*.

[9] Fargas-Marques, A., and Shkel, A. "On electrostatic actuation beyond snapping condition". *IEEE Sensors Conference, Irvine, California, USA, October 31 - November 3 2005*.

[10] Turner, K. L., Miller, S. A., Hartwell, P. G., MacDonald, N. C., Strogatz, S. H., and Adams, S. G., 1998. "Five parametric resonances in a micromechanical system". *Nature,* **vol. 396**, November.

[11] Nayfeh, A. H., and Younis, M. I., 2005. "Dynamics of mems reonators under superharmonic and subharmonic excitations". *IOP Journal of Micromechanics and Microengineering,* **vol. 15**, pp. 1840–1847.

[12] Zhang, W., Baskaran, R., and Turner, K. L., 2002. "Effect of cubic nonlinearity on auto-parametrically amplified resonant mems mass sensor". *Sensors and Actuators A,* **vol. 3578**, pp. 1–11.

[13] Gallacher, B. J., Burdess, J. S., and Harish, K. M., 2006. "A control scheme for a mems electrostatic resonant gyroscope excited using combined parametric excitation and harmonic forcing". *IOP Journal of Micromechanics and Microengineering,* **vol. 16**, pp. 320–331.

[14] Cagdaser, B., Jog, A., Last, M., Leibowitz, B. S., Zhou, L., Shelton, E., Pister, K. S., and Boser, B. E. "Capacitive sense feedback control for mems beam steering mirrors". *Solid-State Sensor, Actuator and Microsystems Workshop, Hilton Head Island, South Carolina, USA, June 6 - 10, 2004*.

[15] Trusov, A., Acar, C., and Shkel, A. M., 2006. "Comparative analysis of distributed mass micromachined gyroscopes fabricated in scs-soi and efab". *Proceedings of SPIE Volume: 6174, Smart Structures and Materials 2006: Sensors and Smart Structures Technologies for Civil, Mechanical, and Aerospace Systems*.

[16] Horowitz, P., and Hill, W., 1989. *The Art of Electronics*. Cambridge University Press.

[17] Cohen, A., Frodis, U., Tseng, F.-G., Zhang, G., Mansfeld, F., and Will, P., 1999. "Efab: low-cost automated electrochemical batch fabrication of arbitrary 3-d microstructures". *SPIE Conference on Micromachining and Microfabrication Process Technology V*.